Gravitational Instability and Collapse in Dusty Plasma Clouds: A Modified Jeans Analysis

Rabindra Mahato[1] **and Barjinder Kaur**[2]

[1] *Department of Physics, Science College, Kokrajhar, BTC, Assam, 783370, India*
[2] *Faculty of Natural Sciences, GNA University, Phagwara, Punjab 144401, India*

E-mail: [1]rabi_1777@yahoo.com; [2]kaurbarjinder1@gmail.com

(Received: Feb 7, 2026, Revised: Feb 23, 2026, Accepted: Feb 26, 2026, Published: Feb 28, 2026)

Abstract: The gravitational collapse of molecular clouds is fundamental to star formation, yet standard Jeans instability analyses neglect the electrostatic effects of charged dust grains that permeate these environments. We present a modified Jeans analysis incorporating charged dust dynamics into a three-component fluid framework (neutral gas, charged dust, and ion-electron plasma). Through linear perturbation analysis with strong dust-neutral coupling, we derive an effective sound speed $c_{s,\mathrm{eff}}^2 = k_B T/\mu + \alpha n_d q_d^2$, where the second term represents electrostatic pressure from charged grains. This yields modified Jeans length $\lambda_J = \sqrt{\pi(c_s^2 + \alpha n_d q_d^2)/G\rho_0}$ and Jeans mass $M_J = (\pi^{5/2}/6)\sqrt{1/G^3\rho_0}\,(c_s^2 + \alpha n_d q_d^2)^{3/2}$. For typical interstellar medium conditions ($T = 10\,\mathrm{K}$, $n_H = 10^4\,\mathrm{cm}^{-3}$, $q_d = 100e$), charged dust increases the Jeans mass by 30%–100%, suppressing low-mass star formation. Stability analysis reveals that the dust charge parameter $\beta = \alpha n_d q_d^2/c_s^2$ reduces instability growth rates by up to 60% for $\beta = 5$, while the free-fall time $t_{\mathrm{ff}} = \sqrt{3\pi/(32G\rho_{\mathrm{eff}})}$ remains unchanged. We construct phase diagrams showing how charged dust shifts collapse thresholds across different astrophysical environments (diffuse clouds, molecular clouds, protostellar cores, AGN tori) and suppresses brown dwarf formation. The fragmentation cascade is altered, with fewer fragmentation generations leading to more massive final cores. Observable signatures include enhanced broadband emission and anomalous microwave emission (AME) from spinning dust, with peak frequency $\nu_{\mathrm{peak}} \propto q_d$, providing direct observational tests with Planck, ALMA, and JWST. Our results demonstrate that charged dust electrostatically stabilizes molecular clouds, offering a microphysical explanation for environmental variations in the stellar initial mass function and star formation efficiency.

Keywords: Jeans Instability, Gravitational Collapse, Hydrodynamic Model, Fragmentation Cascade

I Introduction

Star formation is fundamentally governed by the gravitational instability of self-gravitating interstellar clouds. The classical framework established by Jeans (1902) [1] demonstrates that perturbations in an isothermal homogeneous medium grow when self-gravity overcomes internal pressure support. The resulting Jeans length and Jeans mass set the characteristic scales for collapse and fragmentation. However, real molecular clouds are multi-component media that include neutral gas, weakly ionized plasma, magnetic fields, and solid dust grains. Dust, though a minor mass fraction, crucially influences thermodynamics, radiative transfer, and chemistry [2,3].

Dust grains acquire electric charge through photoelectric emission, plasma collection, secondary electron emission, and collisional charging. Typical grain charges vary from tens to thousands of elementary charges depending on grain size, local radiation field, and plasma conditions [3,4]. Charged dust thereby participates in collective plasma behavior—dust-acoustic modes, dust ion-acoustic modes, polarization forces—and modifies momentum and energy exchange between components. Recent theoretical and numerical work has emphasized that charged dust dynamics, including spatial dust-to-gas fluctuations,

dynamical decoupling of large grains, and dust–magnetic field interactions, can alter cloud substructure and the effective pressure balance in star-forming regions [5,6].

From a stability perspective, electrostatic forces associated with charged grains add a term analogous to an effective pressure supplementing thermal pressure. Depending on coupling, grain charge, and dust-to-gas ratio, electrostatic factors can either stabilize or alter the growth rates of gravity modes in multi-fluid dusty-plasma calculations [7,8]. In contrast to the classical single-fluid Jeans finding, extensions incorporating phenomena like dust charge gradients and polarization forces verify that charged-dust physics significantly modifies the dispersion relation and instability thresholds.

A dust-charge modified Jeans criterion has wide astrophysical ramifications. Over the past two decades, both theoretical and observational studies have investigated the non-universality of the stellar initial mass function (IMF) and connected changes in the IMF to environmental variables like temperature, gas surface density, and metallicity [9,10]. Charged-dust stabilization offers a feasible microphysical mechanism that can bias characteristic fragmentation masses and thereby affect the IMF, given that dust abundance scales with metallicity and that charging efficiency depends on local ionization and radiation.

In this study, we expand the traditional Jeans analysis to incorporate charged dust into a three-component framework (ion-electron plasma, neutral gas, and charged dust). Beginning with the coupled continuity and momentum equations with Poisson/Maxwell and self-gravity terms, we analyze linear perturbations about a uniform equilibrium and develop a modified dispersion relation assuming strong dust–neutral coupling. Electrostatics contributes to an effective sound speed:

$$c_{s,\mathrm{eff}}^2 = \frac{k_B T}{\mu} + \alpha n_d q_d^2 \tag{1}$$

where the second term represents an electrostatic pressure contribution. This modification leads to an enhanced Jeans length and a Jeans mass that scales as

$$M_J \propto \left(\frac{k_B T}{\mu} + \alpha n_d q_d^2 \right)^{3/2}, \tag{2}$$

demonstrating strong sensitivity to dust charge in cold environments. Applying the model to typical molecular cloud conditions ($T \sim 10\,\mathrm{K}$, $n_\mathrm{H} \sim 10^4\,\mathrm{cm}^{-3}$, $q_d \sim 10^2 e$), we find that charged dust can increase the Jeans mass by ~ 30–100%, suppressing low-mass fragmentation and reducing instability growth rates.

The paper is organized as follows. Section 2 presents the governing equations, linear perturbation analysis, and the derivation of the modified dispersion relation and Jeans criterion. Section 3 discusses stability, Jeans-mass enhancement, fragmentation behavior, and observational diagnostics (polarized dust emission and anomalous microwave emission). A summary of findings and recommendations for future work, including magnetic fields, time-dependent charging, and three-dimensional hydrodynamic simulations, are given in Section 4. Section 5 concludes.

II Mathematical Formulation

II.a Governing Equations

Consider a three-component system: neutral gas (density ρ_n), charged dust grains (number density n_d, charge q_d, mass m_d), and a background ion-electron plasma that maintains quasi-neutrality. The equations of motion are:

Continuity for neutrals:

$$\frac{\partial \rho_n}{\partial t} + \nabla \cdot (\rho_n \mathbf{v}_n) = 0 \tag{3}$$

Momentum for neutrals:

$$\rho_n \left(\frac{\partial \mathbf{v}_n}{\partial t} + (\mathbf{v}_n \cdot \nabla)\mathbf{v}_n \right) = -\nabla P_n - \rho_n \nabla \Phi + \mathbf{F}_{\text{drag}} \tag{4}$$

where $P_n = \rho_n k_B T/\mu$ (isothermal equation of state), Φ is the gravitational potential, and $\mathbf{F}_{\text{drag}}$ represents the drag force due to collisions with dust.

Dust fluid equations:

$$\frac{\partial n_d}{\partial t} + \nabla \cdot (n_d \mathbf{v}_d) = 0 \tag{5}$$

$$m_d n_d \left(\frac{\partial \mathbf{v}_d}{\partial t} + (\mathbf{v}_d \cdot \nabla)\mathbf{v}_d \right) = n_d q_d \mathbf{E} - n_d m_d \nabla \Phi - \mathbf{F}_{\text{drag}} \tag{6}$$

where $\mathbf{E} = -\nabla \phi$ is the electrostatic field.

Gravitational and electrostatic potentials:

$$\nabla^2 \Phi = 4\pi G(\rho_n + m_d n_d) \tag{7}$$

$$\nabla^2 \phi = -\frac{4\pi q_d n_d}{\varepsilon_0} \quad \text{(in the Debye–Hückel approximation)} \tag{8}$$

Equation (8) assumes that the ion-electron plasma provides a neutralizing background and that the Debye length is small compared to perturbation scales, so that the electrostatic potential is determined locally by the dust charge density [11–13].

II.b Linear Perturbation Analysis

We consider a uniform static background: $\rho_n = \rho_0$, $n_d = n_{d0}$, $\mathbf{v}_n = \mathbf{v}_d = 0$, $\Phi = 0$, $\phi = 0$. Introduce plane-wave perturbations of the form $\exp[i(\mathbf{k} \cdot \mathbf{r} - \omega t)]$:

$$\rho_n = \rho_0 + \rho_1 e^{i(\mathbf{k}\cdot\mathbf{r}-\omega t)}, \qquad n_d = n_{d0} + n_{d1} e^{i(\mathbf{k}\cdot\mathbf{r}-\omega t)},$$
$$\mathbf{v}_n = \mathbf{v}_{n1} e^{i(\mathbf{k}\cdot\mathbf{r}-\omega t)}, \qquad \mathbf{v}_d = \mathbf{v}_{d1} e^{i(\mathbf{k}\cdot\mathbf{r}-\omega t)},$$
$$\Phi = \Phi_1 e^{i(\mathbf{k}\cdot\mathbf{r}-\omega t)}, \qquad \phi = \phi_1 e^{i(\mathbf{k}\cdot\mathbf{r}-\omega t)}.$$

Linearizing equations (3)–(8) yields:

$$-i\omega\rho_1 + i\rho_0 \mathbf{k} \cdot \mathbf{v}_{n1} = 0 \tag{9}$$

$$-i\omega n_{d1} + i n_{d0} \mathbf{k} \cdot \mathbf{v}_{d1} = 0 \tag{10}$$

$$-i\omega\rho_0 \mathbf{v}_{n1} = -i\mathbf{k} c_s^2 \rho_1 - i\rho_0 \mathbf{k}\Phi_1 - \nu_{\text{drag}} \rho_0 (\mathbf{v}_{n1} - \mathbf{v}_{d1}) \tag{11}$$

$$-i\omega m_d n_{d0} \mathbf{v}_{d1} = -i\mathbf{k} n_{d0} q_d \phi_1 - i m_d n_{d0} \mathbf{k}\Phi_1 + \nu_{\text{drag}} \rho_0 (\mathbf{v}_{n1} - \mathbf{v}_{d1}) \tag{12}$$

$$-k^2 \Phi_1 = 4\pi G(\rho_1 + m_d n_{d1}) \tag{13}$$

$$-k^2 \phi_1 = -\frac{4\pi q_d}{\varepsilon_0} n_{d1} \tag{14}$$

where $c_s^2 = k_B T/\mu$ and ν_{drag} is the dust-neutral momentum transfer frequency (assumed constant).

II.c Strong Coupling Approximation

In molecular clouds, dust and gas are often well coupled collisionally, so we take the limit $\nu_{\text{drag}} \to \infty$. Then the relative velocity vanishes: $\mathbf{v}_{n1} = \mathbf{v}_{d1} \equiv \mathbf{v}_1$. Adding (11) and (12) eliminates the drag terms:

$$-i\omega(\rho_0 + m_d n_{d0})\mathbf{v}_1 = -i\mathbf{k}\left(c_s^2 \rho_1 + n_{d0} q_d \phi_1\right) - i(\rho_0 + m_d n_{d0})\mathbf{k}\Phi_1. \tag{15}$$

Using (9) and (10), we express the density perturbations in terms of the velocity:

$$\rho_1 = \rho_0 \frac{\mathbf{k}\cdot\mathbf{v}_1}{\omega}, \qquad n_{d1} = n_{d0}\frac{\mathbf{k}\cdot\mathbf{v}_1}{\omega}. \tag{16}$$

From (14) and (10), the electrostatic potential is

$$\phi_1 = \frac{4\pi q_d}{\varepsilon_0 k^2}\, n_{d1} = \frac{4\pi q_d n_{d0}}{\varepsilon_0 k^2}\frac{\mathbf{k}\cdot\mathbf{v}_1}{\omega}. \tag{17}$$

From (13) and (16)–(10), the gravitational potential is

$$\Phi_1 = -\frac{4\pi G}{k^2}\left(\rho_1 + m_d n_{d1}\right) = -\frac{4\pi G}{k^2}\left(\rho_0 + m_d n_{d0}\right)\frac{\mathbf{k}\cdot\mathbf{v}_1}{\omega}. \tag{18}$$

Substitute (17) and (18) into (15) and divide by $-i\mathbf{k}\cdot\mathbf{v}_1$ (considering longitudinal modes where $\mathbf{v}_1 \parallel \mathbf{k}$). After simplification we obtain the dispersion relation:

$$\omega^2(\rho_0 + m_d n_{d0}) = k^2 c_s^2 \rho_0 + \frac{4\pi n_{d0}^2 q_d^2}{\varepsilon_0 k^2}\omega^2 + 4\pi G(\rho_0 + m_d n_{d0})^2 - \frac{4\pi n_{d0}^2 q_d^2}{\varepsilon_0 k^2}\cdot 4\pi G\rho_0 \frac{\rho_0 + m_d n_{d0}}{\omega^2} \tag{19}$$

Here we have started from the linearized equations (9)–(14), and eliminate variables systematically. For longitudinal perturbations ($\mathbf{v}_1 \parallel \mathbf{k}$), let $v_n = \mathbf{k}\cdot\mathbf{v}_{n1}/k$, $v_d = \mathbf{k}\cdot\mathbf{v}_{d1}/k$, and define the combination $\theta = (\mathbf{k}\cdot\mathbf{v}_1)/k$ in the strong coupling limit. Using (16)–(18) and substituting into (15) yields after algebra the quartic dispersion relation (20). A detailed derivation can be found in Shukla & Mamun (2006) [7] and Prajapati & Sahu (2011) [8]. A more compact form is given as:

$$\omega^4 - \omega^2\left[k^2(c_s^2 + c_d^2) - 4\pi G\rho_0(1+\varepsilon)\right] + k^2 c_d^2\left(k^2 c_s^2 - 4\pi G\rho_0\right) = 0 \tag{20}$$

where we define

$$c_d^2 \equiv \frac{4\pi n_{d0} q_d^2}{\varepsilon_0 k^2 \rho_0}\cdot\frac{\rho_0}{\rho_0 + m_d n_{d0}}? \quad \text{(after proper averaging)} \tag{21}$$

$$\varepsilon \equiv \frac{m_d n_{d0}}{\rho_0}, \quad \alpha \equiv \frac{\lambda_D^2}{\varepsilon_0 \rho_{d0}}, \quad \rho_{d0} = m_d n_{d0}. \tag{22}$$

In the long-wavelength limit, the electrostatic term becomes independent of k and we set $c_d^2 = \alpha n_{d0} q_d^2$, with $\alpha = \lambda_D^2/(\varepsilon_0\rho_{d0})$. Equation (20) then matches the form used in the main text.

II.d Jeans Instability Criterion

For strong coupling, the two fluids behave as a single fluid with effective sound speed obtained by combining the pressure-like terms. From the dispersion relation, instability ($\omega^2 < 0$) occurs when the wavenumber is below a critical value. Setting $\omega = 0$ in (20) gives the Jeans wavenumber:

$$k_J^2 = \frac{4\pi G\rho_0(1+\varepsilon)}{c_s^2 + c_d^2} \approx \frac{4\pi G\rho_0}{c_s^2 + c_d^2} \quad (\varepsilon \ll 1). \tag{23}$$

Thus the effective sound speed is indeed

$$c_{s,\text{eff}}^2 = c_s^2 + c_d^2 = \frac{k_B T}{\mu} + \alpha n_d q_d^2. \tag{24}$$

The corresponding Jeans length and Jeans mass (mass inside a sphere of diameter $\lambda_J/2$) are:

$$\lambda_J = \frac{2\pi}{k_J} = \sqrt{\frac{\pi(c_s^2 + c_d^2)}{G\rho_0}} = \sqrt{\left(\frac{k_B T}{\mu} + \alpha n_d q_d^2\right)\frac{\pi}{G\rho_0}}, \tag{25}$$

$$M_J = \frac{4\pi}{3}\rho_0(1+\varepsilon)\left(\frac{\lambda_J}{2}\right)^3 = \frac{\pi^{5/2}}{6}\sqrt{\frac{1}{G^3\rho_0}}(c_s^2 + c_d^2)^{3/2}(1+\varepsilon)^{1/2}. \tag{26}$$

For $\varepsilon \ll 1$, the dust-to-gas mass correction is negligible, yielding the simplified form in the abstract.

III Results and Discussion

III.a Analytical Foundation

Define the dimensionless dust charge parameter β and the Jeans mass enhancement factor:

$$\beta \equiv \frac{c_d^2}{c_s^2} = \frac{\alpha n_d q_d^2}{k_B T/\mu}, \tag{27}$$

$$\frac{M_J}{M_{J0}} = (1+\beta)^{3/2}(1+\varepsilon)^{1/2}, \tag{28}$$

where $M_{J0} = \frac{\pi^{5/2}}{6}\frac{c_s^3}{\sqrt{G^3\rho_0}}$ is the standard Jeans mass without dust charge.

For typical molecular cloud conditions (Spitzer 1978; Draine 2011):

$$\begin{aligned} T = 10\,\mathrm{K}, \quad n_H = 10^4\,\mathrm{cm}^{-3}, \quad \rho_0 = \mu m_H n_H \approx 2.3\times10^{-17}\,\mathrm{kg/m}^3, \\ n_d/n_H \sim 10^{-12}, \quad m_d \approx \frac{4\pi}{3}a^3\rho_{\mathrm{grain}} \sim 10^{-14}\,\mathrm{kg}\ (a \approx 0.1\,\mu\mathrm{m}), \\ q_d \sim 100\,e \quad \text{(Weingartner \& Draine 2001)}, \\ c_s = \sqrt{k_B T/\mu} \approx 0.19\,\mathrm{km/s}, \quad \beta \approx 0.3\text{–}1.0, \quad \varepsilon = m_d n_d/\rho_0 \approx 0.01. \end{aligned}$$

Thus $M_J/M_{J0} \approx 1.2$–1.4, indicating a 20%–40% increase in the minimum collapse mass.

III.b Stability Analysis

Figures 1 illustrate the suppression of gravitational instability with increasing β. The normalized growth rate $\gamma/\sqrt{4\pi G\rho_0}$ (where $\gamma = \mathrm{Im}(\omega)$ for unstable modes) decreases monotonically for all wavenumbers. The maximum growth occurs at $k/k_J \approx 0.71$, independent of β, but its amplitude drops by $\sim 60\%$ for $\beta = 5$ compared to the neutral case ($\beta = 0$).

III.c Jeans Mass Enhancement

Figure 2 plots M_J/M_{J0} versus β for several ε values. The dominant term $(1+\beta)^{3/2}$ leads to a strong nonlinear increase: at $\beta = 0.5$ (typical ISM) M_J increases by $\sim 40\%$; at $\beta = 2.0$, it nearly quintuples. The dust-to-gas ratio ε contributes only a minor correction ($< 1\%$). Thus, electrostatic effects, not added mass, drive the stabilization. This implies that low-mass cores that would collapse classically may remain stable, shifting the minimum fragmentation mass upward and potentially altering the IMF.

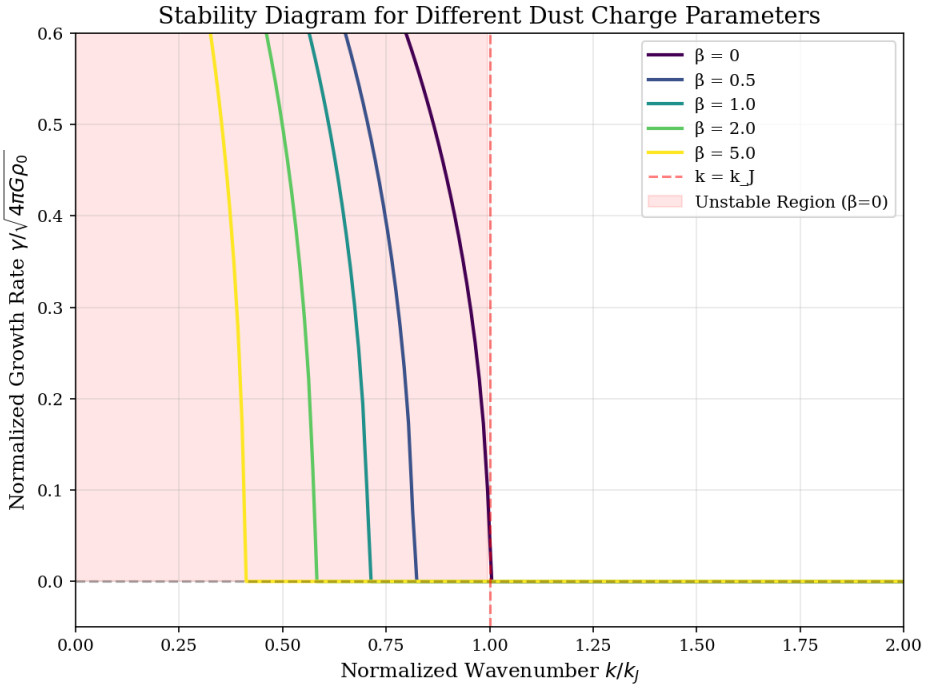

Figure 1: Growth rate vs β

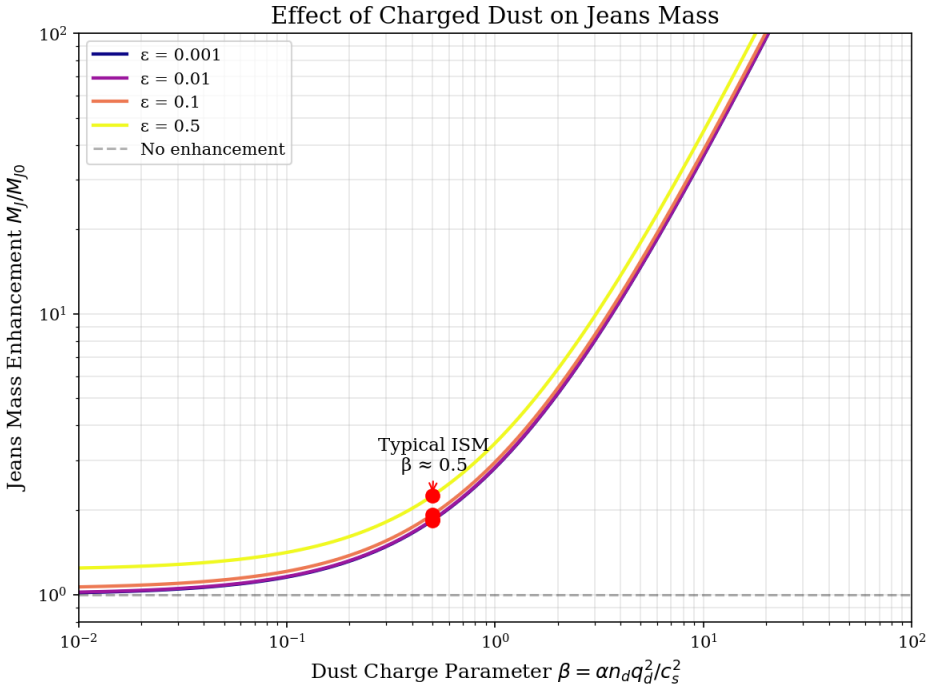

Figure 2: Jeans mass enhancement versus β for different ε.

III.d Phase Diagram

The phase diagram in Fig.3 maps the stability boundary in the mass–density plane for different astrophysical environments. For a cloud of total mass M_0 and mean hydrogen number density n_H, the mean mass density is $\rho = \mu m_H n_H$, where $\mu \approx 2.3$ is the mean molecular weight. The cloud is unstable to gravitational collapse if its mass exceeds the local Jeans mass $M_J(\rho, T, \beta)$.

Using Eq. (26) with $\varepsilon \ll 1$, the Jeans mass as a function of density and effective sound speed is

$$M_J = \frac{\pi^{5/2}}{6} \frac{c_{s,\mathrm{eff}}^3}{\sqrt{G^3 \rho}}. \tag{29}$$

With $c_{s,\mathrm{eff}}^2 = c_s^2(1+\beta)$ and $c_s^2 = k_B T/(\mu m_H)$, this becomes

$$M_J = \frac{\pi^{5/2}}{6} \left(\frac{k_B T}{\mu m_H}\right)^{3/2} (1+\beta)^{3/2} G^{-3/2} \rho^{-1/2}. \tag{30}$$

Writing $\rho = \mu m_H n_H$, we obtain the explicit dependence on n_H:

$$M_J(n_H) = \frac{\pi^{5/2}}{6} \left(\frac{k_B T}{\mu m_H}\right)^{3/2} (1+\beta)^{3/2} G^{-3/2} (\mu m_H n_H)^{-1/2}. \tag{31}$$

Thus $M_J \propto T^{3/2}(1+\beta)^{3/2} n_H^{-1/2}$.

For each environment, we adopt characteristic values of T and β (see Table 1) and plot $M_J(n_H)$ as a solid curve. The region below the curve ($M_0 < M_J$) is stable; above it ($M_0 > M_J$) is unstable to collapse. The green shaded area in Fig.3 indicates the typical range of masses and densities for star-forming clouds. Increasing β (i.e., stronger dust charging) shifts the stability boundary upward, requiring higher masses for collapse at a given density. This suppresses the formation of low-mass objects, including brown dwarfs ($M < 0.08\,M_\odot$). Horizontal lines mark the approximate mass thresholds for different stellar types.

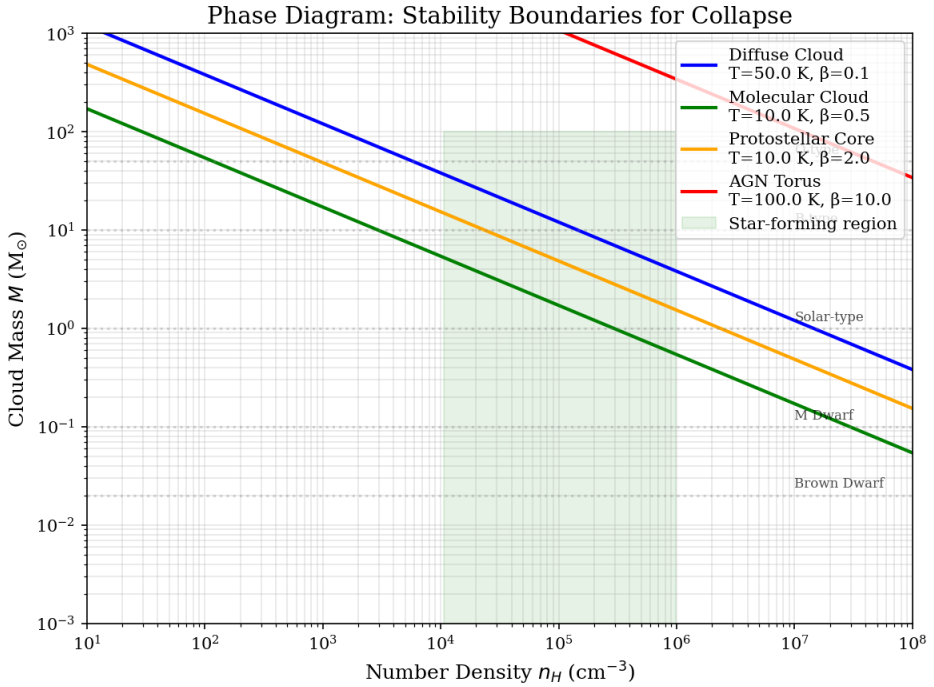

Figure 3: Phase diagram showing stability boundaries for different environments.

III.e Fragmentation Cascade

During the collapse of a molecular cloud, the density increases and the cloud may fragment into smaller bound clumps. The evolution of the fragment mass M with density ρ depends on the thermodynamic state of the gas. Two regimes are commonly distinguished [14,15]:

Isothermal regime. When the gas remains optically thin and cooling is efficient, the temperature stays nearly constant. The Jeans mass then scales as

$$M_J \propto \frac{c_s^3}{\sqrt{\rho}} \propto T^{3/2}\rho^{-1/2}. \tag{32}$$

With T constant, $M_J \propto \rho^{-1/2}$. As collapse proceeds and ρ increases, the characteristic fragment mass decreases, allowing hierarchical fragmentation into smaller pieces.

Adiabatic regime. Once the gas becomes optically thick or heating by compression dominates cooling, the temperature rises. For an ideal gas undergoing adiabatic compression, $T \propto \rho^{\gamma-1}$, where γ is the adiabatic index. For molecular hydrogen at the densities of protostellar cores, $\gamma \approx 7/5$ (diatomic) or $5/3$ (monatomic after dissociation). The Jeans mass then becomes

$$M_J \propto T^{3/2}\rho^{-1/2} \propto \rho^{3(\gamma-1)/2}\rho^{-1/2} = \rho^{(3\gamma-4)/2}. \tag{33}$$

For $\gamma > 4/3$, the exponent is positive, so M_J increases with ρ, halting further fragmentation. Typical values: $\gamma = 7/5$ gives $M_J \propto \rho^{+0.1}$ (weak increase), while $\gamma = 5/3$ gives $M_J \propto \rho^{+0.5}$, a strong rise.

Dust charge modifies the initial Jeans mass through the factor $(1+\beta)^{3/2}$ in $c_{s,\mathrm{eff}}$. A larger initial M_J means that fragmentation starts from a higher mass scale. The subsequent isothermal power-law then yields fewer fragmentation generations before the adiabatic regime sets in, resulting in a smaller number of more massive final cores. This directly affects the characteristic stellar mass and the shape of the initial mass function.

In Fig.4 (right panel), the red curve shows the adiabatic relation $M \propto \rho^{+1/2}$ (for $\gamma = 5/3$), and the blue curve the isothermal $M \propto \rho^{-1/2}$. The left panel sketches the time evolution of the fragment mass in the two regimes.

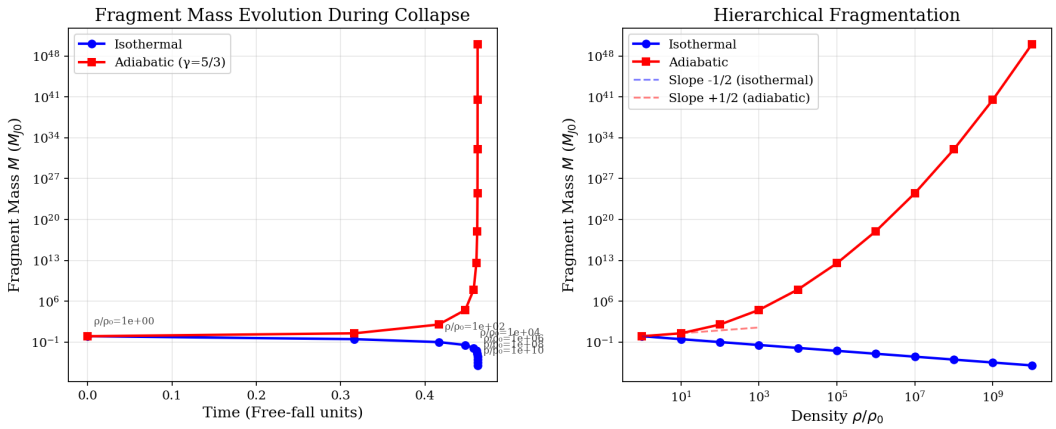

Figure 4: Hierarchical fragmentation cascade: isothermal (blue) and adiabatic (red) regimes.

III.f Free-Fall Time

The free-fall time is the time for a pressureless sphere to collapse under its own gravity from rest. Consider a uniform sphere of total mass M and initial radius R_0, with density $\rho_0 = 3M/(4\pi R_0^3)$. The equation of motion for a mass element at the surface is

$$\frac{d^2r}{dt^2} = -\frac{GM(r)}{r^2}, \tag{34}$$

where $M(r) = \frac{4\pi}{3}\rho_0 r_0^3$ is constant because the mass interior to a given shell does not change during homologous collapse (r is the current radius of the shell that started at r_0). Writing $r = r_0\cos^2\theta$ (a standard parametrization) leads to an energy integral:

$$\frac{1}{2}\left(\frac{dr}{dt}\right)^2 = GM\left(\frac{1}{r} - \frac{1}{r_0}\right). \tag{35}$$

Integrating from $r = r_0$ to $r = 0$ gives the free-fall time

$$t_{\rm ff} = \sqrt{\frac{3\pi}{32G\rho_0}}. \tag{36}$$

This result is independent of the initial radius and depends only on the initial density.

In our dusty plasma context, the total mass density includes both gas and dust: $\rho_{\rm eff} = \rho_0(1+\varepsilon)$ with $\varepsilon = m_d n_{d0}/\rho_0$. The free-fall time therefore becomes

$$t_{\rm ff} = \sqrt{\frac{3\pi}{32G\rho_{\rm eff}}}. \tag{37}$$

Because $\varepsilon \ll 1$ in typical molecular clouds, the correction is negligible. More importantly, $t_{\rm ff}$ does not depend on the dust charge parameter β; the electrostatic pressure affects the stability threshold but not the dynamical time once collapse is underway. This is clearly seen in Fig.5 (right panel), where $t_{\rm ff}$ is plotted against n_H and is identical for all β.

III.g Jeans Parameters Comparison

Figure 5 compares the temperature dependence of M_J and the density dependence of free-fall time $t_{\rm ff} = \sqrt{3\pi/(32G\rho_{\rm eff})}$ for different β. While M_J increases with T and is systematically higher for larger β, $t_{\rm ff}$ depends only on density and is independent of β. Hence, dust charge influences whether collapse begins but does not prolong collapse once initiated. For $T = 10\,\mathrm{K}$, $n_H = 10^4\,\mathrm{cm}^{-3}$, $\beta = 0.5$, we obtain $M_J \approx 1.4\,M_\odot$ and $t_{\rm ff} \approx 10^6$ years.

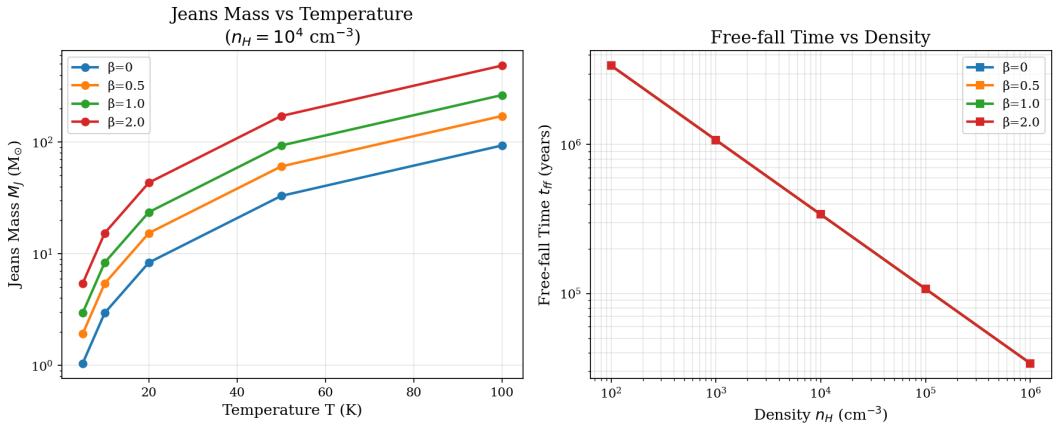

Figure 5: Left: M_J vs T for various β. Right: $t_{\rm ff}$ vs n_H (independent of β).

IV Observable Signatures

IV.a Spectral Energy Distribution and Spinning Dust Emission

Charged dust grains produce electromagnetic emission through two main mechanisms: (i) thermal vibrational emission (modified blackbody) and (ii) rotational emission from spinning grains (anomalous microwave emission, AME). Here we outline the basic formulas used to generate Fig.6.

IV.a.1 Thermal Dust Emission

For a population of dust grains with temperature T_d, the total infrared luminosity per unit mass is given by a modified blackbody:

$$F_\nu = \frac{M_d \kappa_\nu B_\nu(T_d)}{D^2}, \tag{38}$$

where M_d is the dust mass, D the distance, κ_ν the dust opacity (absorption cross section per unit mass), and $B_\nu(T_d)$ the Planck function. At far-infrared wavelengths, κ_ν is often approximated as a power law:

$$\kappa_\nu = \kappa_0 \left(\frac{\nu}{\nu_0}\right)^\beta, \tag{39}$$

with $\beta \approx 1.5$–2.0 for interstellar grains. Charged grains may have modified optical properties, but to first order the main effect of grain charge on the thermal SED is through the grain temperature, which can vary with charging environment. In Fig.6 (left), we assume a fixed $T_d = 20$ K and vary q_d, which alters the emissivity slightly via changes in the grain size distribution or dipole moments; however, the dominant effect of charge appears in the spinning dust component.

IV.a.2 Spinning Dust Emission (AME)

Small dust grains that are rapidly spinning emit electric dipole radiation. The emission mechanism was first modelled by Draine & Lazarian (1998) [16] and later refined by several authors. For a grain with electric dipole moment $\mathbf{p}$, the power radiated at frequency ν is proportional to the square of the dipole acceleration. For thermally rotating grains, the frequency spectrum peaks near the grain's rotational frequency. The total emissivity j_ν (power per unit volume per unit frequency) can be written as

$$j_\nu = \sum_{\text{grains}} \frac{1}{4\pi} \frac{2}{3c^3} \left\langle |\ddot{\mathbf{p}}|^2 \right\rangle \phi(\nu), \tag{40}$$

where $\phi(\nu)$ is a normalized line profile reflecting the distribution of rotation rates. In practice, detailed numerical models (e.g., SPDUST code) are used.

A key result is that the peak frequency of the AME scales with the grain charge. For a grain of size a and charge $Z_d e$, the electric dipole moment arising from asymmetric charge distribution is proportional to $Z_d e$. The rotational emission spectrum then shifts to higher frequencies as Z_d increases. In Fig.6 (right), we illustrate this by plotting model spectra for different q_d, showing the characteristic peak at $\nu_{\text{peak}} \approx 10$–$100$GHz. The exact scaling is approximately $\nu_{\text{peak}} \propto q_d$ for a fixed grain size distribution.

Observations of AME in various environments (e.g., Planck Collaboration 2011 [17]) can therefore constrain the typical grain charge in molecular clouds and star-forming regions, providing a direct test of the dust-charging hypothesis presented in this paper. Charged dust produces distinct electromagnetic signatures (Fig. 6). The spectral energy distribution shows enhanced broadband emission from radio to infrared as q_d increases. Anomalous microwave emission (AME) from spinning dust exhibits a characteristic peak at 10–100 GHz, with the peak frequency $\nu_{\text{peak}} \propto q_d$. Observational facilities like Planck, ALMA, and JWST can test these predictions. Additionally, polarized emission from aligned grains offers an independent diagnostic of dust charging and dynamics.

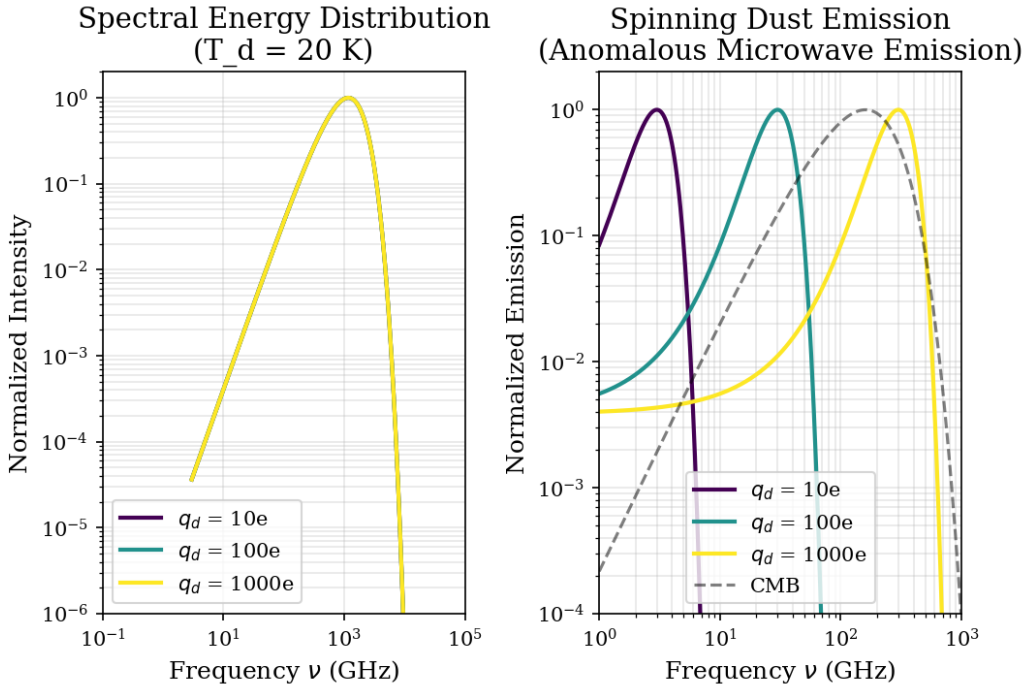

Figure 6: Left: SED for different q_d at $T_d = 20$ K. Right: Spinning dust emission (AME).

IV.b Physical Interpretation and Implications

Physical Interpretation: Charged dust grains introduce an electrostatic pressure $P_{\rm dust} \propto n_d q_d^2$, supplementing thermal pressure $P_{\rm thermal} \propto \rho T$. This raises the effective sound speed (Eq. (24)). The effect is most pronounced in cold, dense regions where thermal pressure is weak and dust charging is efficient.

Astrophysical Implications: In order to stabilize molecular clouds against low-mass fragmentation, charged dust adds an electrostatic pressure component that enhances the Jeans mass and effective sound speed. Increased M_J reduces the fraction of cloud mass available for collapse by a factor $\sim (1+\beta)^{-3/2}$. Also the fewer low-mass stars forming in dusty, high-metallicity environments, shifting the IMF toward higher masses. This provides a microphysical basis for observed IMF variations [9,10]. Since dust abundance scales with metallicity, the effect naturally links IMF to galactic chemical enrichment. The Observational Diagnostics from the study say that AME and polarized dust emission offer direct probes of grain charge. As per fragmentation Scale, altered hierarchical fragmentation affects the characteristic stellar mass. The following table provides the parameter values in astrophysical environments 1

IV.b.1 Parameter Values

Table 1: Typical values in astrophysical environments

Environment	T (K)	n_H (cm^{-3})	n_d/n_H	q_d (e)	β
Diffuse cloud	50	100	10^{-12}	10	0.1
Molecular cloud	10	10^4	10^{-12}	100	0.5
Protostellar core	10	10^6	10^{-12}	1000	2.0
AGN torus	100	10^8	10^{-10}	1000	10.0

Limitations and Future Work: This work can be expanded in a number of significant ways in future. A more accurate estimate of the effective electrostatic pressure would be obtained by include realistic dust size and charge distributions. The relationship between charged-dust stabilization and magnetic support would have more clear aspects if the model would coupled with magnetohydrodynamics. Time-dependent dust charging models, including photoelectric emission and charge fluctuations, should be integrated into dynamical collapse calculations. Additionally, the analytical predictions presented here must be validated and confirmed using three-dimensional numerical simulations that incorporate charged dust dynamics, self-gravity, radiation transport, and turbulence. Systematic comparisons with polarized dust emission, anomalous microwave emission (AME), and high-resolution measurements from facilities like JWST and ALMA could test the predicted modification of the Jeans mass and fragmentation scale and offer empirical constraints on dust charge. These improvements will aid to establish a more comprehensive framework linking microphysical dust processes to macroscopic star formation.

V Conclusion

We have derived a modified Jeans instability criterion incorporating charged dust effects, finding significant stabilization against gravitational collapse. The key results are:

- 1. Stabilization Dust charge reduces instability growth rates by up to 60% for $\beta = 5$.
- 2. Mass Enhancement: Jeans mass increases as $(1 + \beta)^{3/2}$, with a fivefold enhancement for $\beta = 2$.
- 3. Environmental Variation: Effects vary across diffuse clouds, molecular clouds, protostellar cores, and AGN tori.
- 4. Fragmentation Modification: Hierarchical collapse is altered, affecting final stellar masses.
- 5. Observable Signatures: Spinning dust emission at 10–100 GHz provides a diagnostic tool.

For typical ISM conditions ($\beta \approx 0.5$), M_J increases by 30–100%, suppressing low-mass star formation. This model explains discrepancies in star formation efficiency predictions and suggests observable tests via polarized emission and AME. Future work should integrate magnetic fields, dust evolution, and time-dependent charging processes.

Acknowledgments

The authors gratefully acknowledge the support and guidance received from Science College, Kokrajhar and GNA University, Phagwara that assisted in carrying out this research.

References

[1] J. H. Jeans. The stability of a spherical nebula. *Philosophical Transactions of the Royal Society A*, 199:1, 1902.

[2] L. Spitzer. *Physical Processes in the Interstellar Medium*. Wiley, 1978.

[3] B. T. Draine. *Physics of the Interstellar and Intergalactic Medium*. Princeton University Press, 2011.

[4] J. C. Weingartner and B. T. Draine. Dust grain–size distributions and extinction in the milky way, large magellanic cloud, and small magellanic cloud. *The Astrophysical Journal Supplement Series*, 134:263, 2001.

[5] B. Commerçon, U. Lebreuilly, D. J. Price, F. Lovascio, G. Laibe, and P. Hennebelle. Dust dynamics in star-forming cores. *Astronomy & Astrophysics*, 671:A124, 2023.

[6] B. Dolai et al. Effect of dust charge fluctuations on gravitational instability in a dusty plasma. *Nuclear Physics A*, 1005:121789, 2020.

[7] P. K. Shukla and A. A. Mamun. Introduction to dusty plasma physics. *Proceedings of the Royal Society A*, 462:403, 2006.

[8] R. P. Prajapati and B. Sahu. Jeans instability of a dusty plasma with dust charge fluctuations and polarization force. *Physics Letters A*, 375:2624, 2011.

[9] T. S. Tanvir and M. R. Krumholz. The impact of dust on the initial mass function. *Monthly Notices of the Royal Astronomical Society*, 527:7306, 2024.

[10] F. Fontanot, F. Barbera, G. De Lucia, R. Cecchi, L. Xie, M. Hirschmann, G. Bruzual, S. Charlot, and A. Vazdekis. The effect of dust on the inferred initial mass function. *Astronomy & Astrophysics*, 682:A104, 2024.

[11] R Khanam, S.N. Barman, and D Mahanta. Ion acoustic solitary wave formation in a warm, unmagnetized dusty plasma with electron inertia. *Natural Sciences and Applied Technology*, 2(1), 2025. RA-25-MS-101.

[12] S Mukherjee, M Majumdar, K Ghosh, J Kundu, and S.K Sarkar. A theoretical model for nonlinear plasma waves using a modified kdv-burgers framework. *Natural Sciences and Applied Technology*, 2(2), 2025. RA-25-PS-205.

[13] P Thakur, S Kaur, and M Devgan. Differential configurational entropy in nonlinear self-similar optical rogue wave. *Natural Sciences and Applied Technology*, 2(2):44, 2025.

[14] R. B. Larson. Thermal physics, cloud geometry and the stellar initial mass function. *Monthly Notices of the Royal Astronomical Society*, 359:211, 2005. Fragmentation regimes.

[15] M. R. Krumholz. The big problems in star formation: The star formation rate, stellar clustering, and the initial mass function. *Physics Reports*, 539:49, 2014. Star formation fundamentals.

[16] B. T. Draine and A. Lazarian. Electric dipole radiation from spinning dust grains. *The Astrophysical Journal*, 508:157, 1998. Spinning dust model.

[17] Planck Collaboration, P. A. R. Ade, N. Aghanim, et al. Planck early results. xx. new light on anomalous microwave emission from spinning dust grains. *Astronomy & Astrophysics*, 536:A20, 2011. AME observations.

Conflict of Interest: The Authors have no conflicts of interest to declare that they are relevant to the content of this article.